https://doi.org/10.15407/ufm.25.04.765

V.A. DEKHTYARENKO [1,2,*], T.V. PRYADKO [1,], T.P. VLADIMIROVA [1,***], C.V. MAKSYMOVA [2,****], O.M. SEMYRGA [1,*****], and V.I. BONDARCHUK [1,******]**

[1] G.V. Kurdyumov Institute for Metal Physics of the N.A.S. of Ukraine, 36 Academician Vernadsky Blvd., UA-03142 Kyiv, Ukraine
[2] E.O. Paton Electric Welding Institute of the N.A.S. of Ukraine, 11 Kazymyr Malevych Str., UA-03150 Kyiv, Ukraine

* devova@i.ua, ** pryadko@imp.kiev.ua,
*** tvlad@imp.kiev.ua, angelsgift@ukr.net, **** maksymova.svitlana15@ukr.net,
***** o_semyrga@ukr.net, ****** vbondar77@gmail.com

EFFECT OF ALLOYING ON THE HYDROGEN SORPTION IN Ti–Zr–Mn-BASED ALLOYS. Pt. 2: Eutectic Alloys with Laves Phase and B.C.C. Solid-Solution Structure

After reviewing and analysing literature data, the microstructure and phase composition of the $Ti_{47.5}Zr_{28}Mn_{(22.5-x)}V_2Ni_x$ (where x = 5.0 and 17.5 at.%) eutectic alloys in the as-cast and annealed states as well as the phase composition of the hydrogenation products of these alloys are investigated using the x-ray phase analysis and scanning electron microscopy methods. As found, nickel is distributed in the alloy between the b.c.c. solid solution and the intermetallic compound with a significantly higher content in the latter. In addition, the phase composition of the initial alloy is changed with the substitution of Mn by 5.0–17.5 at.% of Ni: the ternary NiTiZr ψ-phase, which is isostructural to the Laves phase ($C14$), is formed. As shown, the size of the intermetallic crystallites is a critical factor for the activation of the H absorption at room temperature and a hydrogen pressure of 0.6 MPa. At a grain surface area of 1–10 μm^2 in the initial eutectic microstructure, active interaction of the alloy with hydrogen at the first hydrogenation occurs exclusively during the heating and isobaric–isothermal exposure at 510 ± 10 °C, whereas this process starts at room temperature, when the

Citation: V.A. Dekhtyarenko, T.V. Pryadko, T.P. Vladimirova, C.V. Maksymova, O.M. Semyrga, and V.I. Bondarchuk, Effect of Alloying on the Hydrogen Sorption in Ti–Zr–Mn-Based Alloys. Pt. 2. Eutectic Alloys with Laves Phase and B.C.C. Solid-Solution Structure, *Progress in Physics of Metals*, **25**, No. 4: 765–786 (2024)

area of the crystallites is increased up to 100–300 μm² after annealing. An increase in the size of each of the phase components cause greater volume misfits at the interphase boundaries between the adjacent crystallites at the initial stages of hydrogenation that leads to the cracking of the alloy surface and subsequent activation of interaction with hydrogen.

Keywords: nickel, eutectic, b.c.c. solid solution, intermetallic compound, hydrogenation, dehydrogenation, hydrogen capacity.

1. Introduction

Even though the hydrogen sorption properties of the alloys based on the AB_2 intermetallic compound (*C*14-type Laves phase) have been studied since the end of the 70s of the last century [1, 2] and until now [3–6], the theoretical value of hydrogen capacity 3.9 wt.% [7] has not been achieved yet. One of the possible ways to solve this problem is the selection of a complex of alloying elements. However, it was shown on an example of $TiMn_2$ intermetallic compound that the transition from the binary Ti–Mn system [8–10] to more complex alloying systems with up to 6 components [11, 12] allowed increasing the amount of absorbed hydrogen by a maximum of 20% (≈2.10 wt.%); at the same time, the kinetics of sorption–desorption processes was significantly deteriorated in some cases. In addition, alloy production is extremely complicated due to the different melting points of the components.

Therefore, some researchers [13, 14] assumed that a significant increase in the amount of absorbed hydrogen and, what is especially important, the preservation of the favourable parameters of the sorption–desorption kinetics in the alloys based on the AB_2 intermetallic compound can be achieved using a more complex approach which consists in deviation from the stoichiometric AB_2 composition with simultaneous alloying and changing the general phase and structural state of the material.

The authors of [13, 14] studied the hydrogen sorption properties of the alloys of the Ti–V–Mn and Ti–Zr–Mn–V systems based on the AB_2 intermetallic compound and showed that there was a certain amount of Ti-based b.c.c. solid solution rather often, together with the Laves phase. For quite a long time, it was believed [15–18] that the presence of even a small amount of this Ti-based b.c.c. phase in the alloys based on the AB_2 intermetallic compound deteriorates the kinetic parameters of hydrogen sorption–desorption, since this phase has a technologically complicated preliminary thermal activation, a low rate of hydrogenation even at fairly high temperatures of 400–600 °C, and a relatively high-temperature range of desorption [19, 20].

However, as shown in Refs. [13, 14], the process of hydrogen sorption in these alloys was single-stage, *i.e.*, multiphase alloys interacted with hydrogen as single-phase ones. Thus, it was proved that the b.c.c. solid solu-

tion in coexistence with the AB_2 intermetallic compound could interact with hydrogen under thermobaric conditions typical for the hydrogenation of the intermetallic compound. It was also shown that it was possible to change the amount of absorbed hydrogen in a fairly wide range by varying the volume fractions of the AB_2 intermetallic compound and b.c.c. solid solution in two-phase alloys [13, 14, 21, 22]. Therefore, the authors of Refs. [13, 14] first proposed a new concept for developing materials with a high hydrogen capacity, namely, 'Laves phase-related b.c.c. solid solution'.

Based on previous studies [13, 14], we proposed another approach to the development of hydrogen-sorbent materials with the structure comprised of the AB_2 intermetallic compound and the b.c.c. solid solution [23]. For the first time, it was proposed to use the eutectic alloys (natural composites) with monovariant $L \approx \beta(\text{Ti}) + (\text{Zr,Ti})\text{Mn}_2$ eutectic transformation as hydrogen-sorbent materials.

We showed in the example of the $\text{Ti}_{47.5}\text{Zr}_{30}\text{Mn}_{22.5}$ alloy [23] that the condition of the minimum possible manganese content in the AB_2-type intermetallic compound is automatically fulfilled during the eutectic solidification of the melt (the necessity of the minimum possible Mn content in the alloys based on the TiMn_2 intermetallic compound was shown in Ref. [10]). Due to the eutectic solidification, a system of interphase boundaries with a high specific surface also formed in the alloy. This contributed to the fast kinetics of hydrogenation, since, as known from the literature [24], a high rate of hydrogen infiltration into the bulk material is provided by its diffusion along grain boundaries. In addition, the eutectic solidification allowed the stabilizing of the Ti-based b.c.c. solid solution in this alloy at room temperature, which is important for interaction with hydrogen. The hydrogen capacity of the Ti-based β-phase is 4 wt.% [7], while it is only 0.01 wt.% for the α-phase [25]; meanwhile, the hydrogen diffusion coefficient in the β-phase is 3.5 times higher than in the α-phase [26].

The hydrogen sorption properties of the $\text{Ti}_{47.5}\text{Zr}_{30}\text{Mn}_{22.5}$ alloy were studied at room temperature and a hydrogen pressure of 0.6 MPa. It was shown [23] that this alloy can interact with hydrogen at room temperature and the above-mentioned pressure at a high rate; however, this requires activation heating during the first hydrogenation up to 520 °C with subsequent desorption of hydrogen. Such a high amount of absorbed hydrogen as 2.58 wt.% (62.6 at.% H) was reached, which corresponded to the formula composition $\text{H}/Me \approx 1.64$, whereas the hydrogen capacity did not exceed 2.10 wt.% ($\text{H}/Me \approx 1.38$) for the alloys based on the AB_2 intermetallic compound [27, 28].

In Refs. [29–36], the studies of eutectic alloys based on the Ti–Zr–Mn system with the structure comprised of AB_2 intermetallic compound and b.c.c. solid solution was expanded. The effect of changes in the initial structure (the ratio of volume fractions of constituent phases) and/or phase composition (transition from the Laves phase of the *C*14-to-*C*15

Table 1. **Nominal compositions of the alloys**

Alloy			Composition, at.%				
			Ti	Zr	Mn	V	Ni
1	Ni-0	$Ti_{47.5}Zr_{28}Mn_{22.5}V_2$	47.5	28	22.5	2	—
2	Ni-5	$Ti_{47.5}Zr_{28}Mn_{17.5}V_{25}Ni_5$	47.5	28	17.5	2	5
3	Ni-17.5	$Ti_{47.5}Zr_{28}Mn_5V_2Ni_{17.5}$	47.5	28	5	2	17.5

type) on the kinetics of the hydrogenation-dehydrogenation processes in the first cycle and the amount of absorbed hydrogen was determined. In addition, it was shown that preliminary heat treatment (annealing) allowed initiating active absorption of hydrogen by the alloys of this type at room temperature [34]. However, the ever-increasing requirements for materials used as hydrogen sorbents (operating time of a hydrogen battery on one charge) require further improvement of already developed materials, *i.e.*, the search for elements for their additional alloying. Based on the literature data [7, 37], it was found that nickel can be a promising element for additional alloying since it can form a stable chemical compound with hydrogen [38], as well as dissolve in the Laves phases of the above-mentioned type [11].

The purpose of this research was to enhance the hydrogen capacity and improve the kinetics of hydrogen sorption–desorption processes in the eutectic alloys of the Ti–Zr–Mn–V system using their additional alloying with nickel and preliminary heat treatment.

The perspective of the chosen approach can be confirmed by a comparison of the hydrogen sorption properties of new Ni-modified alloys with those of the previously studied $Ti_{47.5}Zr_{28}Mn_{22.5}V_2$ alloy whose structure, phase composition, and properties in the as-cast state and after heat treatment were investigated in detail in [32–34] (Table 1). When choosing alloy compositions for research, it was fundamental to preserve their eutectic structure.

2. Materials and Experimental Techniques

The samples of the alloys (Table 1) with weights up to 30 g were melted in a KPTM-2 laboratory electric arc furnace with a non-consumable tungsten electrode on a water-cooled copper base in a protective atmosphere. The charge was remelted up to 5 times to achieve high homogenization of the ingots. The following materials were used as starting components: iodide titanium (99.95%), iodide zirconium (99.975%), electrolytic manganese (99.9%), electrolytic vanadium (99.5%), and electrolytic nickel (99.5%) [at.%].

The alloys were annealed in a SNVL-1.3.1/16M2 furnace at 800 °C (exposure time 16 hours) at a pressure of 10^{-3} Pa (heating rate 20 °C/min)

to study the microstructure evolution and to remove residual stresses that formed during solidification and mechanical processing of the ingots. The isothermal annealing temperature was chosen based on previous studies [34] to provide the maximum rate of diffusion of the alloy components and prevent its melting.

X-ray phase studies were carried out at a DRON-3M diffractometer with monochromatic CuK_α radiation.

Metallographic studies were carried out at a VEGA3 TESCAN scanning electron microscope equipped with an XFlash610M (Bruker) EDX detector.

The hydrogen sorption properties of the alloys were studied by the Sieverts technique at an IVGM-2M unit under a hydrogen pressure of 0.6 MPa at room temperature or during heating at a rate of 0.125 °C/s and isobaric and isothermal exposure at 520 °C (see [39, 40] for the details). The hydrogen desorption process was also investigated at an IVGM-2M unit under an initial pressure of 0.0002 MPa.

The amount of absorbed or released hydrogen was determined by the change in pressure in a closed volume before and after the experiment (volumetric method) and was additionally controlled by weighing on VLR-20 scales with an accuracy of 1.5×10^{-5} g (gravimetric method). Labyrinth-like crucibles were used to prevent sample mass loss during vacuuming, as well as the infiltration of various impurities into the hydrogenation products during experiments.

To confirm the reliability of the obtained results, studies were carried out on several samples of the same composition. This paper presents the results for only the first cycle of sorption–desorption.

3. Results and Discussion

3.1. Structure and Phase Composition of Alloys

The phase compositions of the alloys were studied by x-ray phase analysis and using MAUD software (distributed without license restrictions as public domain) (Table 2). The phase composition of the alloy chosen as a base [33, 34] included the hexagonal Laves λ-phase of the *C*14 type ($P6_3/mmc$ space group of $MgZn_2$ structural type) and b.c.c. solid solution ($1m$–$3m$ space group of W structural type). The diffractograms of the experimental $Ti_{47.5}Zr_{28}Mn_{17.5}V_2Ni_5$ and $Ti_{47.5}Zr_{28}Mn_5V_2Ni_{17.5}$ alloys, in addition to the phases mentioned above, contained the reflections of another compound isostructural to the Laves phase of the *C*14 type with slightly different lattice constants (Fig. 1). According to the Crystallography Open Database of cif-files, the reflections of the NiTiZr ψ-phase (ternary Laves phase of the $MgZn_2$ type) were identified [41]. It should be noted that alloying with nickel changed not only the phase composition of the base alloy but also the ratio of phase fractions. In the base alloy [33, 34], according to MAUD software, the b.c.c. solid solution/λ-phase ratio was 0.598/0.402. Alloying

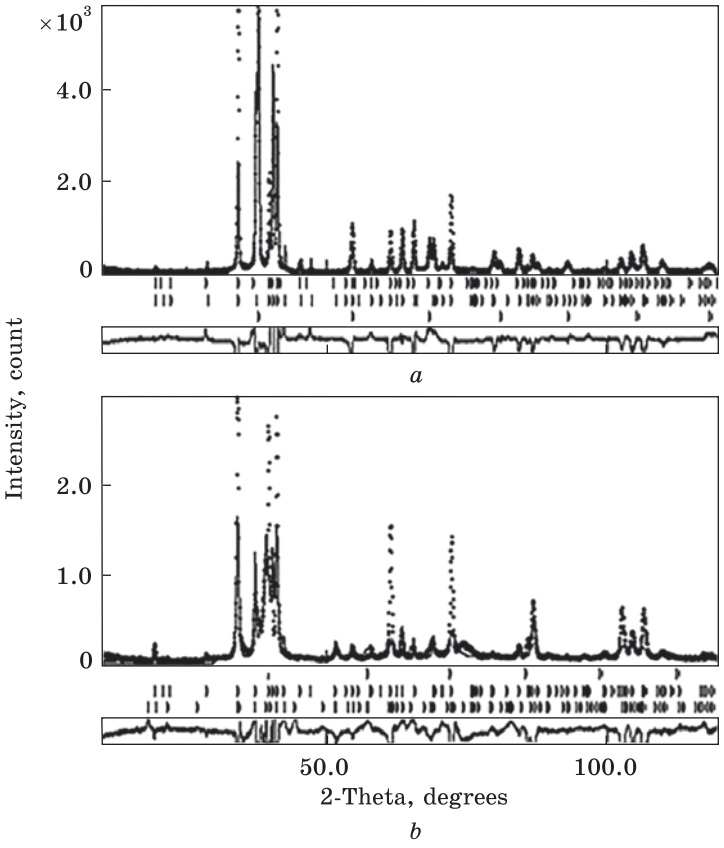

Fig. 1. Diffractograms of the experimental as-cast $Ti_{47.5}Zr_{28}Mn_{17.5}V_2Ni_5$ (*a*) and $Ti_{47.5}Zr_{28}Mn_5V_2Ni_{17.5}$ (*b*) alloys

Table 2. **Lattice constants of phases in as-cast state and after heat treatment (h.t.)**

Alloy	State	Lattice constants ±0.0009, nm		
		l-phase	b.c.c.	NiTiZr ψ-phase
Ni-0	as-cast	$a = 0.5200$ $c = 0.8581$	$a = 0.3352$	—
	after h.t.	$a = 0.5195$ $c = 0.8534$	$a = 0.3365$	—
Ni-5	as-cast	$a = 0.5224$ $c = 0.8476$	$a = 0.3354$	$a = 0.5226$ $c = 0.8657$
	after h.t.	$a = 0.5223$ $c = 0.8439$	$a = 0.3352$	$a = 0.5427$ $c = 0.8520$
Ni-17.5	as-cast	$a = 0.5195$ $c = 0.8641$	$a = 0.3214$	$a = 0.5226$ $c = 0.8504$
	after h.t.	$a = 0.5225$ $c = 0.8421$	$a = 0.3214$	$a = 0.5253$ $c = 0.8476$

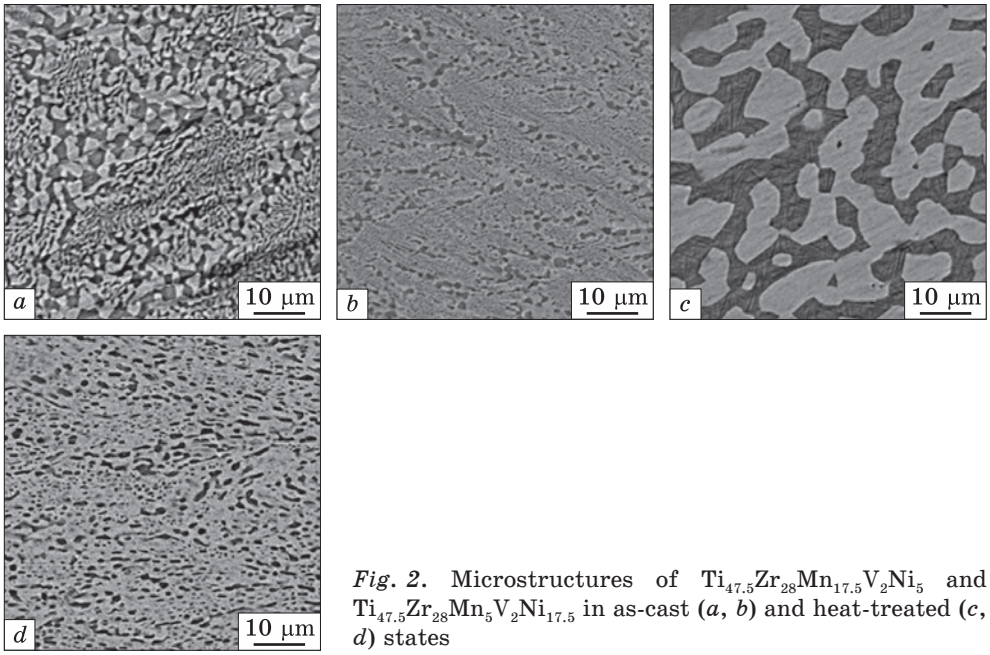

Fig. 2. Microstructures of $Ti_{47.5}Zr_{28}Mn_{17.5}V_2Ni_5$ and $Ti_{47.5}Zr_{28}Mn_5V_2Ni_{17.5}$ in as-cast (*a*, *b*) and heat-treated (*c*, *d*) states

with nickel led to a significant decrease in the volume fraction of the b.c.c. solid solution: 0.476/0.504 with the fraction of the ψ-phase 0.020 in the $Ti_{47.5}Zr_{28}Mn_{17.5}V_2Ni_5$ alloy; 0.463/0.492 with the fraction of the ψ-phase 0.045 in the $Ti_{47.5}Zr_{28}Mn_5V_2Ni_{17.5}$ alloy.

Examination of the samples using scanning electron microscopy showed that the partial substitution of manganese with nickel, despite changes in the phase composition, did not significantly affect the microstructure of the alloy (Fig. 2, *a*, *b*). The microstructure remained eutectic. As in the base alloy, the eutectic consisted of solid solution and intermetallic compound, and had a skeletal-like structure, where the intermetallic compound particles acted as nucleation sites for eutectic solidification (this phase formed the framework of the colonies). This is confirmed by the curving of intermetallic fibres at the junctions of adjacent eutectic colonies. Since the growth of eutectic colonies generates heat, which crucially reduces the cooling rate, it is accompanied by a transition from a fibrous structure to the formation of globules at the ends of the fibres. The controlled phase is the solid solution that forms the matrix of the colonies. Thus, the phase that initiates and controls the eutectic solidification is the phase with a higher enthalpy of melting, as in most solid solution/intermetallic compound systems. The formation of the framework of the eutectic colony and its further growth is typical for polyhedron-dendrite eutectics.

Therefore, alloying with nickel in the above concentration range allows for preserving the eutectic structure with an extremely branched

system of interphase boundaries with a high specific surface area, and minimizing the manganese content in the intermetallic compound to enhance the hydrogen sorption properties [10, 42, 43].

The chemical compositions of the phases were determined, which allowed the identification of these phases (bright-coloured crystallites correspond to intermetallic compound), and the distribution of nickel in the $Ti_{47.5}Zr_{28}Mn_{22.5}V_2$ alloy [33, 34] was studied using scanning electron microscopy and EDX spectroscopy (Table 3). A comparison of the obtained results with similar data for the original $Ti_{47.5}Zr_{28}Mn_{22.5}V_2$ eutectic alloy made it possible to conclude that the alloying with nickel is accompanied by the distribution of this element between the b.c.c. solid solution and the intermetallic compound, with higher Ni content in the latter. The presence of nickel in the b.c.c. solid solution significantly reduces manganese content in this phase: from ≈10.91 at.% in the original alloy (without Ni) to ≈2.03 at.% in the $Ti_{47.5}Zr_{28}Mn_5V_2Ni_{17.5}$ alloy. The alloying also made it possible to lower the manganese content in the AB_2 intermetallic compound with the average content of the B component at the appropriate level. According to the literature [44–48], the substitution of manganese, which does not interact with hydrogen, with elements which form a stable chemical compound with hydrogen leads to an enhancement in hydrogen absorption properties (an increase in hydrogen capacity). In the $Ti_{47.5}Zr_{28}Mn_5V_2Ni_{17.5}$ alloy, the chemical composition of the bright crystallites corresponds to the ternary ψ-phase NiTiZr. The average content of B component (≈27.88 at.%) in this case is fully consistent with the data of [41]; according to this work, the ψ-phase exists in the range of concentrations from ≈14 to ≈34 at.% of Zr and from ≈25 to ≈39 at.% of Ni.

Table 3. **Chemical compositions of phases**

Alloy	State	Crystallites	Composition, at.%				
			Ti	Zr	Mn	V	Ni
Ni-0	as-cast	Bright	38.36	28.84	30.14	2.66	—
		Dark	60.05	27.65	10.91	1.39	—
	after h.t.	Bright	28.95	27.94	36.78	5.75	—
		Dark	70.80	22.27	5.03	1.90	—
Ni-5	as-cast	Bright	38.97	27.30	23.52	1.27	8.94
		Dark	65.13	27.00	5.47	1.13	1.26
	after h.t.	Bright	37.27	26.71	26.76	1.56	7.70
		Dark	71.11	24.11	3.25	1.12	0.41
Ni-17.5	as-cast	Bright	44.96	27.16	3.65	1.23	23.00
		Dark	63.85	24.91	2.03	1.14	8.07
	after h.t.	Bright	47.69	25.75	5.69	1.44	19.44
		Dark	68.56	21.14	2.41	1.11	6.78

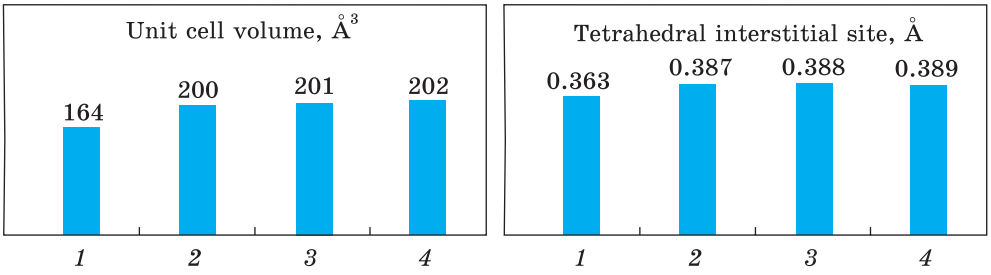

Fig. 3. Volume of unit cell and radius of the tetrahedral interstitial site of *C*14 Laves phase in alloys: *1* — $TiMn_2$ [52]; *2* — $Ti_{47.5}Zr_{28}Mn_{22.5}V_2$ [32–34]; *3* — $Ti_{47.5}Zr_{28}Mn_{17.5}V_2Ni_5$; *4* — $Ti_{47.5}Zr_{28}Mn_5V_2Ni_{17.5}$

Studies of the evolution of the microstructure (Fig. 2, *c*, *d*) and the phase compositions after the above-mentioned heat treatment showed that the coagulation of the structural components occurred during annealing, *i.e.*, the microstructure coarsened due to the consolidation of the phase components and the formation of rather large phase clusters. Using the ImageJ software (distributed without license restrictions as public domain), it was determined that the grain areas in the $Ti_{47.5}Zr_{28}Mn_{17.5}V_2Ni_5$ alloy increased from 1–10 μm^2 in the as-cast state to 100–300 μm^2 after 16 hours of annealing (Fig. 2, *a*, *c*). At the same time, the specific surface area of the interphase boundaries decreased by 10–15 times. In addition, the fraction of the b.c.c. solid solution decreased from 0.476 to 0.431, and the lattice constants of the phases changed (Table 2) due to the redistribution of chemical components between the phases (Table 3), which differ significantly in atomic radii [49]. The same samples were examined before and after annealing; the results were averaged over several sections of the ingots.

In the $Ti_{47.5}Zr_{28}Mn_5V_2Ni_{17.5}$ alloy, the coagulation of the eutectic structure also occurred during annealing, but this did not lead to a significant increase in the grain areas of the phases. In this alloy, the fraction of b.c.c. solid solution also decreased from 0.463 to 0.370, and the lattice constants of the phases changed (Table 2) due to the redistribution of chemical components between the phases (Table 3).

The annealing and the corresponding redistribution of chemical components had the most effect on the ternary ψ-phase NiTiZr. Its volume fraction increased from 0.020 to 0.052 in the $Ti_{47.5}Zr_{28}Mn_{17.5}V_2Ni_5$ alloy and from 0.045 to 0.110 in the $Ti_{47.5}Zr_{28}Mn_5V_2Ni_{17.5}$ alloy.

Based on the results of x-ray phase analysis and the data of [50, 51], the volume of the unit cell of the Laves phase and the radius of the tetrahedral interstitial site for Ni-modified alloys were calculated (Fig. 3). The calculations were carried out for as-cast state only for the A_2B_2 interstitial sites, since, according to [50, 51], dissolved hydrogen occupies only these sites in the Laves phase of the *C*14 type. A comparison of the obtained

data with those for the binary compound $TiMn_2$ [52] shows that the chemical composition of the nickel-modified alloys provides a larger volume of the unit cell (by 22.5–23.1%), and a larger radius of the tetrahedral interstitial site (by 6.9–7.1%). According to the literature [50, 51], this should have a positive effect on the total amount of hydrogen absorbed by the alloy.

3.2. Kinetics of Interaction of Alloys with Hydrogen

Regardless of the state (as-cast or annealed), the process of interaction of nickel-modified alloys with hydrogen, as well as the base $Ti_{47.5}Zr_{28}Mn_{22.5}V_2$ alloy, was started at room temperature and a hydrogen pressure of 0.6 MPa. Exposure of as-cast alloys for 24 hours under these conditions did not lead to surface activation and, accordingly, to active absorption. It was assumed that the inactivated state of the surface prevents intensive hydrogen sorption, so a longer incubation period is required. However, increasing the exposure time up to 48 hours also did not initiate the hydrogenation process. The lack of active absorption of hydrogen by as-cast alloys at room temperature is presumably explained by the insufficient surface area of intermetallic crystallites. Active absorption of hydrogen was only observed during heating (Fig. 4) and upon isobaric and isothermal exposure at 510±10 °C. The interaction with hydrogen began at 170±10 °C, but the reaction rate was very low. To accelerate the interaction, the temperature was increased to the above-mentioned range. The temperatures T_{abs} were determined from the dependence $P = f(T)$ (Fig. 4); these temperatures to a certain extent depend on the Ni content in the alloy (Table 4).

Taking into account the temperatures of the beginning of active absorption for Ni-modified alloys (345 °C and 450 °C), it can be stated that the hydrogenation process in them (as well as in the base alloy [33]) begins in the Ti-based b.c.c. solid solution. This conclusion is based on the literature data: according to the results of Refs. [53–55], titanium and Ti-based b.c.c. solid solution actively interacts with hydrogen exactly in the temperature range of 400–600 °C, and the process of dihydride formation takes several hours due to a rather low rate of interaction. Most likely, the beginning of the process of active absorption of hydrogen at the above-

Table 4. **Kinetic parameters of hydrogenation and hydrogen capacity**

Alloy	State	T_{abs}, °C	τ_{inc}, min	τ_{hyd}, min	c_H, wt.%	H/*Me*
Ni-0	as-cast	395	—	15	2.66	1.67
	after h.t.	20	180	150	2.65	1.67
Ni-5	as-cast	345	—	15	2.70	1.70
	after h.t.	20	120	120	2.65	1.68
Ni-17.5	as-cast	450	—	30	2.70	1.72
	after h.t.	20	115	110	2.70	1.72

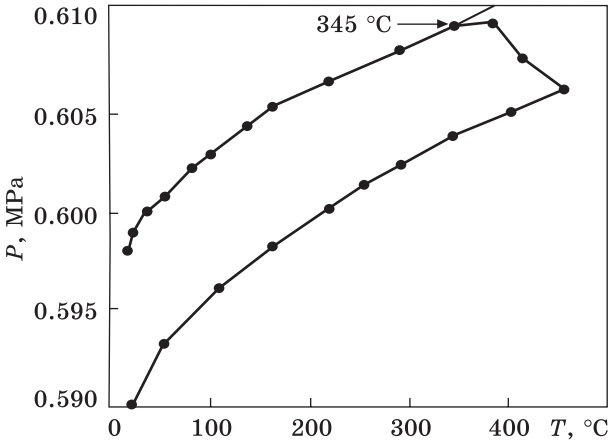

Fig. 4. Dependence of the hydrogen pressure on the temperature during the first hydrogenation of $Ti_{47.5}Zr_{28}Mn_{17.5}V_2Ni_5$ alloy

mentioned temperatures (400–600 °C) is associated with the cracking and failure of the oxide scale, which is always present on the surface of titanium and acts as a barrier to the infiltration of hydrogen into the material. The discontinuity and, accordingly, a larger volume of the δ-hydride formed compared to the initial b.c.c. solid solution leads to the formation of cracks, which not only crush the material throughout the sample bulk but also form new surfaces that are free from oxide scale, facilitating the activation of the intermetallic compound and contributing to its rapid saturation.

Comparing the amount of hydrogen absorbed by the base $Ti_{47.5}Zr_{28}Mn_{22.5}V_2$ alloy [33] and nickel-modified alloys (in the as-cast state), one can conclude that an increase in the radius of the tetrahedral interstitial site in the Laves phase and the total amount of the elements that interact with hydrogen led to a higher total hydrogen capacity (Table 4).

To confirm that the size of the intermetallic crystallites affects the activation of hydrogen absorption during the first hydrogenation, the hydrogen absorption properties of the annealed alloys were also investigated at room temperature and a hydrogen pressure of 0.6 MPa for 24 hours (Fig. 5). A significant increase in the area of intermetallic grains on the surface enabled the hydrogenation process of the annealed alloys at room temperature. However, the smaller length of the interphase boundaries increased the hydrogenation time (Table 4), as the hydrogen diffusion coefficient is approximately 10^3 times higher along

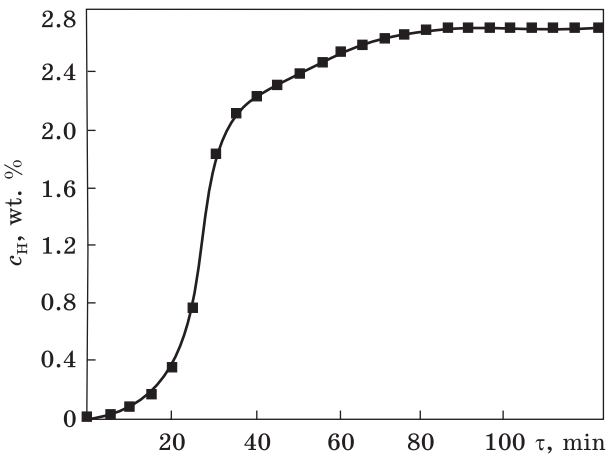

Fig. 5. Dependence of the absorbed hydrogen concentration on the time of the first hydrogenation for annealed $Ti_{47.5}Zr_{28}Mn_5V_2Ni_{17.5}$ alloy

the grain boundaries than in the volume. However, it should be noted that the alloying with nickel led to a decrease in both the incubation period and the time needed for the saturation by hydrogen.

Since hydrogen absorption began at room temperature, surface activation occurred due to the uncompensated interatomic bonds in the intermetallic compound. As a result, the dissociation of hydrogen molecules was facilitated, which caused rapid infiltration of hydrogen atoms into the intermetallic matrix with subsequent migration along the interphase boundaries. This is consistent with the data of [34, 56], where it was noted that the hydrogenation process at room temperature began exactly on intermetallic crystallites in a multiphase structure. A significant increase in the volume of the intermetallic unit cell (by 15–25% according to [57]) leads to its destruction and the formation of a surface free of oxide scale not only on the intermetallic crystallites but also on the b.c.c. solid solution, involving the latter in the process of hydrogenation at room temperature.

Similar to the base $Ti_{47.5}Zr_{28}Mn_{22.5}V_2$ alloy, the saturation with the hydrogen of nickel-modified eutectic alloys of the Ti–Zr–Mn–V–Ni system led to the disintegration of solid samples into a powder regardless of the initial state (as-cast or annealed).

The phase composition and lattice constants of the final product of the hydrogenation of the alloys were investigated by x-ray phase analysis and MAUD software (Table 5, Fig. 6).

Regardless of the initial state of the alloys (as-cast or annealed) and the conditions of the hydrogenation (room temperature or heating), hydrogenation products were based on the initial phases. These products were δ-hydride with an f.c.c.-lattice formed based on the b.c.c.-solid solution,

Table 5. **Lattice constants of phases after hydrogenation**

Alloy	State	Lattice constants ±0.0009, nm			H/*Me*	H/*Me*		
		λ-phase	δ-hydride	ψ-phase		λ-phase	δ-hydride	ψ-phase
Ni-0	as-cast	a = 0.5572 c = 0.9152	a = 0.4438		1.67	1.30	2.03	—
	h.t.	a = 0.5567 c = 0.9145	a = 0.4433		1.67	1.32	1.98	—
Ni-5	as-cast	a = 0.5575 c = 0.9070	a = 0.4540	a = 0.5383 c = 0.8725	1.70	1.26	2.24	0.81
	h.t.	a = 0.5594 c = 0.9121	a = 0.4501	a = 0.5592 c = 0.9052	1.68	1.37	2.13	0.80
Ni-17.5	as-cast	a = 0.5581 c = 0.9047	a = 0.4825	a = 0.5600 c = 0.9120	1.72	1.31	2.23	1.34
	h.t.	a = 0.5596 c = 0.9100	a = 0.4515	a = 0.5525 c = 0.9949	1.72	1.37	2.20	1.32

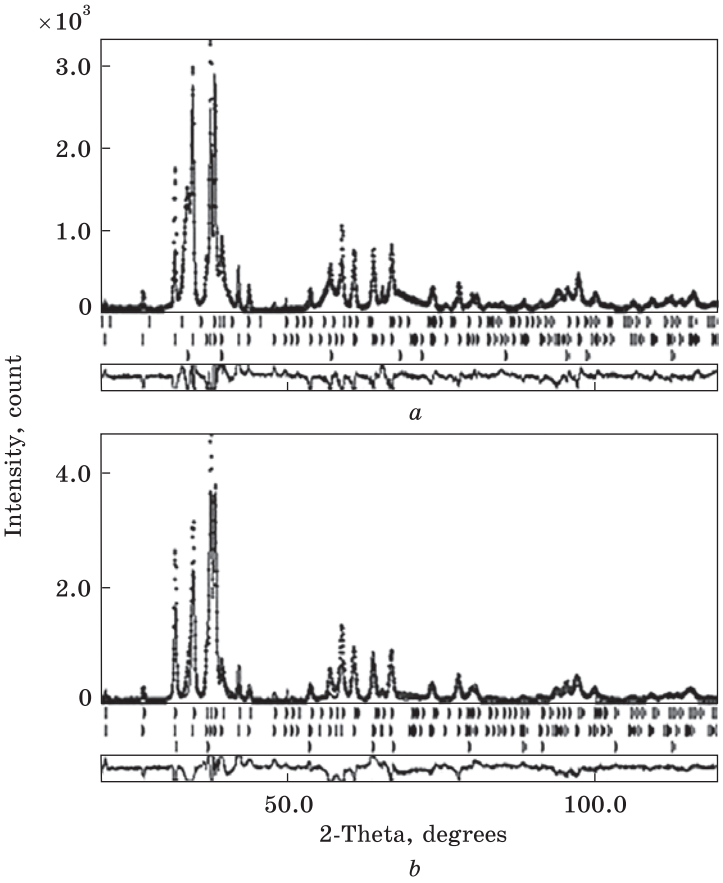

Fig. 6. Diffractograms of the hydrogenated as-cast $Ti_{47.5}Zr_{28}Mn_{17.5}V_2Ni_5$ (*a*) and $Ti_{47.5}Zr_{28}Mn_5V_2Ni_{17.5}$ (*b*) alloys

and λ-(TiZr)Mn_2–H and ψ-NiTiZr–H hydrides based on the Laves phases (see Table 5 and Fig. 6).

The interaction of nickel-modified alloys with hydrogen resulted in an extremely significant increase in the fraction of the ψ-NiTiZr-H phase: from 0.020 to 0.104 and from 0.052 to 0.202 in the $Ti_{47.5}Zr_{28}Mn_{17.5}V_2Ni_5$ alloy, from 0.045 to 0.201 and 0.110 to 0.250 in the $Ti_{47.5}Zr_{28}Mn_5V_2Ni_{17.5}$ alloy in as-cast and annealed state, respectively. Generally, this is consistent with [58] regarding the fact that hydrogen treatment of some metals makes it possible to control the formation of the phase composition and microstructure, stabilize the high-temperature phase, lower the critical temperature of the phase transformation, to realize recrystallization, to change the conditions of ageing and decomposition (or ordering [59–61]) of metastable phases, *etc*.

To evaluate the hydrogen capacity of the b.c.c. solid solution and the Laves phase separately, the ratio of their volume fractions was determined using the data of x-ray phase analysis and MAUD calculations. The amount of hydrogen in all hydrides based on the Laves phase was calculated ac-

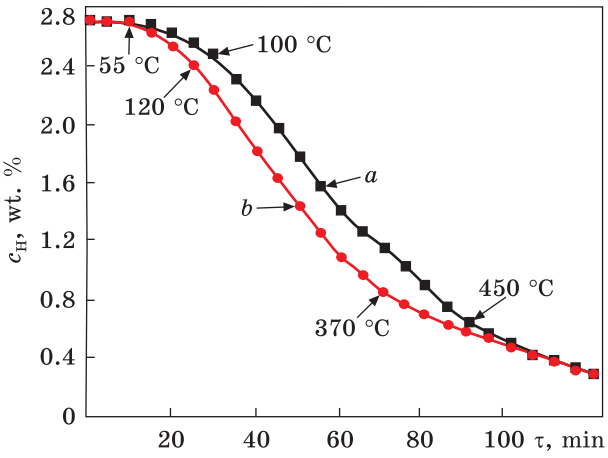

Fig. 7. Changes in hydrogen capacity during hydrogen desorption of alloys: (*a*) $Ti_{47.5}Zr_{28}Mn_{17.5}V_2Ni_5$ and (*b*) $Ti_{47.5}Zr_{28}Mn_5V_2Ni_{17.5}$ (as-cast state)

cording to Ref. [62]: the increase in the unit cell volume is $2.9 \cdot 10^{-3}$ nm^3 per unit of H/*M*, where *M* is the number of metal atoms in the unit cell (the Pearson symbol for the $MgZn_2$-type structure is *hP*12). The calculated increase in the volume of the unit cell of the Laves phase per one metal atom made it possible to evaluate the hydrogen capacity of intermetallic compounds and to connect the residual amount of absorbed hydrogen with the δ-hydride based on the b.c.c. solid solution.

The results listed in Table 5 indicate that the alloying with nickel enhanced the hydrogen capacity of both the alloys and the b.c.c. solid solution. It should be noted that the Ti-based solid solution absorbed hydrogen with kinetics similar to that of the intermetallic compound; a high hydrogen capacity was reached at room temperature. This is largely due to the b.c.c. lattice of the β-phase solid solution, where the hydrogen diffusion coefficient at room temperature is almost two orders of magnitude higher compared to the α-phase with an h.c.p. lattice. A mild decrease in the hydrogen capacity of some Laves phases is most likely caused by the presence of two isostructural components. Taking into account the average volume fraction of hydrides based on the λ- and ψ-phase, the total amount of absorbed hydrogen is $H/Me \approx 1.33$.

It can be stated that the main reason for the increase in the hydrogen capacity of the b.c.c. solid solution is the significant decrease in Mn content (Table 3), as was mentioned above. The obtained result confirms previous data [47, 48] on the positive effect of partial substitution of manganese (which does not form hydrides) by elements, which interact with hydrogen.

According to the literature [33, 34], the release of hydrogen at an initial pressure in the chamber of 0.0002 MPa from hydrogenation products of the base $Ti_{47.5}Zr_{28}Mn_{22.5}V_2$ alloy begins at ≈60 °C, regardless of the initial state (as-cast or annealed). Upon heating to 300 °C, ≈50% of the absorbed hydrogen was released, and almost 100% reversible capacity was achieved, when the temperature was increased up to 500 °C.

The process of hydrogen release from hydrogenation products formed during hydrogen saturation of nickel-modified alloys (in as-cast state) was studied at an initial pressure of 0.0002 MPa. At a heating rate of 3 °C/min,

the active hydrogen release began at 55±5 °C (Fig. 7), and this process involved three stages. At the first stage (from 55 °C to 110±10 °C), the hydrogen release was relatively slow, only 10% of the absorbed hydrogen was released. The average release rate at this stage was ≈0.0065 and ≈0.0096 wt.%/min for the $Ti_{47.5}Zr_{28}Mn_{17.5}V_2Ni_5$ and $Ti_{47.5}Zr_{28}Mn_5V_2Ni_{17.5}$ alloy, respectively. Starting from 110±10 °C, the average rate of hydrogen release increased to ≈0.031 and ≈0.035 wt.%/min for the $Ti_{47.5}Zr_{28}Mn_{17.5}V_2Ni_5$ and $Ti_{47.5}Zr_{28}Mn_5V_2Ni_{17.5}$ alloy, respectively. When the temperature reached 370 °C for the $Ti_{47.5}Zr_{28}Mn_{17.5}V_2Ni_5$ alloy and 450 °C for the $Ti_{47.5}Zr_{28}Mn_5V_2Ni_{17.5}$ alloy, 68 and 76% of the total amount of absorbed hydrogen were released, respectively. Above these temperatures, the average release rate decreased in both alloys to ≈0.012 wt.%/min, and the amount of released hydrogen increased to 90% up to 490±10 °C. At this temperature, an additional operation was applied, namely, pumping out the released hydrogen that provided almost 100% reversible capacity.

Since an important property of the alloys for hydrogen storage is the preservation of hydrogen sorption parameters during multiple cycles of hydrogen sorption–desorption, this aspect was studied for nickel-modified alloys. As mentioned above, a significant reduction in the length of grain boundaries after annealing does not affect the hydrogen capacity of multiphase alloys; nevertheless, this factor affects the kinetic parameters of hydrogenation at the first stage. However, the initial grain size of the intermetallic crystallites no longer affected the incubation period and the rate of hydrogenation after the first sorption–desorption cycle due to the complete crushing of the samples; further, the surface area of new particles and the absence of oxide scale on them played the main role. After sorption–desorption cycling, the alloys had activated surfaces and were able to absorb hydrogen at room temperature and a pressure of 0.2 MPa, *i.e.* three times lower than during the first hydrogenation (0.6 MPa), starting from the first seconds of contact with a hydrogen environment with an average rate of $2–4\times10^{-3}$ wt.%/s. Although the hydrogen capacity did not change, the time to reach its maximum value was reduced significantly. The hydrogenation pressure was reduced to show the enhancement of hydrogen sorption properties already after the first sorption–desorption cycle whose main role was to activate the material. The possibility to saturate the alloys with hydrogen at a low pressure makes the hydrogenation process safer, and the hydrogen batteries lighter (there is no need to use massive containers), which is especially important for practical applications in transport [63].

This enhancement of the hydrogen sorption properties of nickel-modified alloys during the second cycle can be explained by the following factors: (i) the material activation after the first cycle of hydrogen sorption–desorption; (ii) crushing of the samples with an increase in the specific surface area [64, 65]; (iii) a reduction in oxygen content on the surface

and in the volume of hydride particles as a result of oxygen interaction with desorbed hydrogen atoms released upon the first desorption [66, 67].

4. Conclusions

Partial substitution of manganese (which does not interact with hydrogen) by hydride-forming nickel resulted in enhanced hydrogen capacity of the alloys. This is explained by the simultaneous action of several factors: preservation of the eutectic structure; increased size of tetrahedral interstitial sites in the Laves phase; and an increase in the total amount of the hydride-forming element both in the alloy and in each phase component.

Heat treatment of eutectic alloys led to the coagulation of eutectic structure and positively affected hydrogen sorption properties by lowering the hydrogenation temperature to room temperature. Surface activation occurred due to the increased surface area of crystallites with uncompensated interatomic bonds in the Laves phase. As a result, the dissociation of hydrogen molecules was facilitated, which caused rapid infiltration of hydrogen atoms into the intermetallic matrix with their subsequent diffusion along the interphase boundaries. The coarsening of each phase component also caused greater volume misfits at the interphase boundaries between neighbouring crystallites, which led to the cracking and crushing of the material. As a result, new juvenile surfaces appeared that led to further activation of the interaction with hydrogen not only in the intermetallic compound but also in the b.c.c. solid solution, involving the latter in the hydrogenation process at room temperature.

The first cycle of hydrogen sorption–desorption of eutectic alloys, regardless of their phase and structural state and the conditions of the first hydrogenation process, is an effective way of activating materials for their further use as hydrogen accumulators. Due to the complete crushing of the samples during hydrogen sorption, the size of the initial intermetallic grains no longer affected the incubation period and the rate of hydrogenation. The surface area of new particles and the absence of oxide scale dissolved by atomic hydrogen upon desorption played the main role. The alloys after the sorption–desorption cycle had highly activated surfaces, so they were able to absorb hydrogen at room temperature and a pressure of 0.2 MPa starting from the first seconds of contact with a hydrogen environment at an average rate of $2–4\times10^{-3}$ wt.%/s. Although the hydrogen capacity did not change, the time to reach its maximum value was significantly reduced.

Acknowledgement. The work was carried out as a part of the research work ‘Effect of phase and structural states of Ni- and Ti-based eutectic alloys on their physical and mechanical properties’ for 2020–2024 (State Reg. No. 0120U103313).

REFERENCES

1. D. Shaltiel, I. Jacob, and D. Davidov, Hydrogen Absorption and Desorption Properties of AB_2 Laves-Phase Pseudobinary Compounds, *J. Less-Common Met.*, **53**: 117–131 (1977);
https://doi.org/10.1016/0022-5088(77)90162-X
2. D.P. Shoemaker and C.B. Shoemaker, Concerning Atomic Sites and Capacities for Hydrogen Absorption in the AB_2 Friauf-Laves Phases, *J. Less-Common Met.*, **68**: 43–58 (1979);
https://doi.org/10.1016/0022-5088(79)90271-6
3. M. Piao, X. Xiao, L. Zhan, Z. Cao, P. Zhou, J. Qi, M. Lu, Z. Li, L. Jiang, F. Fang, and L. Chen, Laves Phase Double Substitution Alloy Design and Device Filling Modification for Ti-Based Metal Hydride Hydrogen Compressors, *Int. J. Hydrogen Energy*, **50**: 1358–1368 (2024);
https://doi.org/10.1016/j.ijhydene.2023.09.228
4. V.A. Dekhtyarenko, Hydrogen-Sorption Properties of the Alloy $Ti_{15.5}Zr_{30}Mn_{38}V_{5.5}Cr_{5.5}Co_{5.5}$ Based on the Laves Phase (Type *C*14), *Metallofiz. Noveishie Tekhnol.*, **45**, No. 6: 743–755 (2023);
https://doi.org/10.15407/mfint.45.06.0743
5. X. Zhang, B. Li, L. Wang, W. Xiong, J. Li, S. Zhou, J. Xu, Y. Zhao, X. He, and H. Yan, Hydrogen Storage Properties of AB_2 Type Ti–Zr–Cr–Mn–Fe Based Alloys, *Int. J. Hydrogen Energy*, **51**: 193–201 (2024);
https://doi.org/10.1016/j.ijhydene.2023.11.045
6. V.A. Dekhtyarenko, T.V. Pryadko, T.P. Vladimirova, S.V. Maksymova, H.Yu. Mykhailova, and V.I. Bondarchuk, Effect of Alloying on the Hydrogen Sorption in Ti–Zr–Mn-Based Alloys. Pt. 1: *C*14-Type Laves-Phase-Based Alloys, *Prog. Phys. Met.*, **25**, No. 3: 520–544 (2024);
https://doi.org/10.15407/ufm.25.03.520
7. V.A. Dekhtyarenko, D.G. Savvakin, V.I. Bondarchuk, V.M. Shyvanyuk, T.V. Pryadko, and O.O. Stasiuk, $TiMn_2$-Based Intermetallic Alloys for Hydrogen Accumulation: Problems and Prospects, *Prog. Phys. Met.*, **22**, No. 3: 307–351 (2021);
https://doi.org/10.15407/ufm.22.03.307
8. J.L. Bobet, B. Chevalier, and T.B. Darrie, Crystallographic and Hydrogen Sorption Properties of $TiMn_2$ Based Alloys, *Intermettallics*, **8**, No. 4: 359–363 (2000);
https://doi.org/10.1016/S0966-9795(99)00092-8
9. J.L. Bobet and T.B. Darriet, Relationship Between Hydrogen Sorption Properties and Crystallography for $TiMn_2$ Based Alloys, *Int. J. Hydrogen Energy*, **25**: 767–772 (2000);
https://doi.org/10.1016/S0360-3199(99)00101-9
10. S. Samboshi, N. Masahashi, and S. Hanada, Effect of Composition on Hydrogen Absorbing Properties in Binary $TiMn_2$ Based Alloys, *J. Alloys Compd.*, **352**: 210-217 (2003);
https://doi.org/10.1016/S0925-8388(02)01125-8
11. P. Liu, X. Xie, L. Xu, X. Li, and T. Liu, Hydrogen Storage Properties of $(Ti_{0.85}Zr_{0.15})_{1.05}Mn_{1.2}Cr_{0.6}V_{0.1}M_{0.1}$ (M = Ni, Fe, Cu) Alloys Easily Activated at Room Temperature, *Prog. Nat. Sci.*, **27**: 652–657 (2017);
https://doi.org/10.1016/j.pnsc.2017.09.007
12. Z. Cao, L. Ouyang, H. Wang, J. Liu, L. Sun, and M. Zhu, Composition Design of Ti–Cr–Mn–Fe Alloys for Hybrid High-Pressure Metal Hydride Tanks, *J. Alloys Compd.*, **639**: 452–457 (2015);
https://doi.org/10.1016/j.jallcom.2015.03.196

13. H. Iba and E. Akiba, Hydrogen Absorption and Modulated Structure in Ti–V–Mn Alloys, *J. Alloys Compd.*, **253–254**: 21–24 (1997); https://doi.org/10.1016/S0925-8388(96)03072-1
14. E. Akiba and H. Iba, Hydrogen Absorption by Laves Phase Related BCC Solid Solution, *Intermetallic*, **6**: 461–470 (1998); https://doi.org/10.1016/S0966-9795(97)00088-5
15. J. Huot, D.B. Ravnsbæk, J. Zhang, F. Cuevas, M. Latroche, and T.R. Jensen, Mechanochemical Synthesis of Hydrogen Storage Materials, *Prog. Mater. Sci.*, **58**: 30–75 (2013); https://doi.org/10.1016/j.pmatsci.2012.07.001
16. C. Raufast, D. Plante, and S. Miraglia, Investigation of the Structural and Hydrogenation Properties of Disordered Ti–V–Cr–Mo BCC Solid Solutions, *J. Alloys Compd.*, **617**: 633–638 (2014); https://doi.org/10.1016/j.jallcom.2014.07.089
17. N. Skryabina, D. Fruchart, M.G. Shelyapina, S. Dolukhanyan, and A. Aleksanyan, Phase Transformations in Ti–V Hydrides, *J. Alloys Compd.*, **580**: S94–S97 (2013); https://doi.org/10.1016/j.jallcom.2013.03.114
18. H. Itoh, H. Arashima, K. Kubo, T. Kabutomori, and K. Ohnishi, Improvement of Cyclic Durability of BCC Structured Ti–Cr–V Alloys, *J. Alloys Compd.*, **404–406**: 417–420 (2005); https://doi.org/10.1016/j.jallcom.2004.12.175
19. G.G. Libowitz and A. Maeland, Hydride Formation by B.C.C. Solid Solution Alloys, *Mater. Sci. Forum*, **30**: 177–196 (1988); https://doi.org/10.4028/www.scientific.net/MSF.31.177
20. S. Ono, K. Nomura, and J. Ikeda, The Reaction of Hydrogen with Alloys of Vanadium and Titanium, *J. Less-Common. Met.*, **72**: 159–165 (1980); https://doi.org/10.1016/0022-5088(80)90135-6
21. V.G. Ivanchenko, V.A. Dekhtyarenko, and T.V. Pryadko, Sorption Properties of Heterophase Alloys β(Ti,Zr,Mn)+(Ti,Zr)Mn_{2-x}, *Metallofiz. Noveishie Tekhnol.*, **33**, Spec. Iss.: 479–484 (2011) (in Russian).
22. V. Dekhtyarenko, T. Pryadko, and O. Boshko. Effect of the Phase Composition of the Ti–Zr–Mn–V Alloys on the Interaction Kinetics with Hydrogen, *Chem. Met. Alloys*, **11**, No. 3/4: 77–84 (2018); https://doi.org/10.30970/cma11.0371
23. V. Ivanchenko, T. Pryadko, V. Dekhtyarenko, and T. Kosorukova, Hydrogen Absorbing Properties of a Ti–Zr–Mn Eutectic Alloy, *Chem. Met. Alloys.*, **1**, No. 2: 133–136 (2008); https://doi.org/10.30970/cma1.0044
24. A. Zuttel, Materials for Hydrogen Storage, *Mater. Today*, **6**, No. 9: 24–33 (2003); https://doi.org/10.1016/S1369-7021(03)00922-2
25. O.M. Ivasishin, O.B. Bondarchuk, and M.M. Gumenyak, Surface Phenomena During Heating of Titanium Hydride Powder, *Phys. Chem. Solid State*, **12**, No. 4: 900–907 (2011) (in Ukrainian).
26. *Gases and Carbon in Metals. Pure and Applied Metallurgy in Individual Representations* (Eds. E. Fromm and E. Gebhardt) (Berlin–Heidelberg–New York: Springer Verlag: 1976), vol. **26**; https://doi.org/10.1002/bbpc.19770810821
27. V.A. Dekhtyarenko, Alloy Based on Intermetallic (Ti,Zr)$(V,Mn,Cr)_{2-x}$ Obtained Using Titanium Sponge for Hydrogen Sorption, *Metallofiz. Noveishie Tekhnol.*, **41**, No. 10: 1283–1290 (2019); https://doi.org/10.15407/mfint.41.10.1283

28. V.A. Dekhtyarenko, Hydrogen Storage Properties of $Ti_{15.4}Zr_{30.2}Mn_{44}V_{5.4}Cr_5$ Alloy Produced by Induction and Arc Melting, *Metallofiz. Noveishie Tekhnol.*, **43**, No. 8: 1053–1063 (2021);
https://doi.org/10.15407/mfint.43.08.1053
29. V.G. Ivanchenko, V.A. Dekhtyarenko, and T.V. Pryadko, Variations of the Parameters of Hydrogenation for Alloys of the Ti–Zr– Mn System with 20 at.% Zr Depending on the Structure, *Metaloznav. Obrob. Met.*, No. 1: 4–7 (2010) (in Ukrainian).
30. V.A. Dekhtiarenko, The Influence of Vanadium Addition on Hydrogen Capacity and Absorption–Desorption Kinetics of the Eutectic Ti–Zr–Mn Alloy, *Metallofiz. Noveishie Tekhnol.*, **36**, No. 3: 375–381 (2014) (in Russian);
https://doi.org/10.15407/mfint.36.03.0375
31. V.A. Dekhtyarenko, T.V. Pryadko, D.G. Savvakin, and V.I. Bondarchuk, Structure, Phase Composition, and Hydrogen Absorption Properties of Multiphase Alloys of Ti–Zr–Mn–V System Alloyed with Holmium, *Metallofiz. Noveishie Tekhnol.*, **44**, No. 7: 913–926 (2022);
https://doi.org/10.15407/mfint.44.07.0913
32. V.G. Ivanchenko, V.A. Dekhtyarenko, T.V. Pryadko, and V.I. Nychyporenko, Influence of V on the Structure and Phase Composition of Eutectic $Ti_{0.475}Zr_{0.3}Mn_{0.225}$ Alloy, *Metallofiz. Noveishie Tekhnol.*, **36**, No. 6: 803–813 (2014) (in Russian);
https://doi.org/10.15407/mfint.36.06.0803
33. V.G. Ivanchenko, V.A. Dekhtyarenko, and T.V. Pryadko, Hydrogen Sorption Properties of $Ti_{0.475}Zr_{0.3}Mn_{0.225}$ Eutectic Alloy Alloyed with 2 at.% and 5 at.% of Vanadium, *Metallofiz. Noveishie Tekhnol.*, **37**, No. 4: 521–530 (2015);
https://doi.org/10.15407/mfint.37.04.0521
34. V.G. Ivanchenko, V.A. Dekhtyarenko, T.V. Pryadko, D.G. Savvakin, and I.K. Evlash, Influence of Heat Treatment on the Hydrogen-Sorption Properties of $Ti_{0.475}Zr_{0.3}Mn_{0.225}$ Eutectic Alloy Doped with Vanadium, *Mater. Sci.*, **51**: 492–499 (2016);
https://doi.org/10.1007/s11003-016-9867-7
35. T.V. Pryadko, V.A. Dekhtyarenko, K.M. Khranovs'ka, and H.S. Mohyl'nyi, Influence of the Substitution of Chromium for Manganese on the Structure and Hydrogen-Sorption Properties of $Ti_{47.5}Zr_{30}Mn_{22.5}$ Eutectic Alloy, *Mater Sci.*, **55**: 854–862 (2020);
https://doi.org/10.1007/s11003-020-00379-0
36. V.A. Dekhtyarenko, T.V. Pryadko, D.G. Savvakin, and T.A. Kosorukova, Structure, Phase Composition and Hydrogen Adsorption Properties of Eutectic Alloys of the Ti–Zr–Mn–V System, *Metallofiz. Noveishie Tekhnol.*, **41**, No. 11: 1455–1468 (2019) (in Russian);
https://doi.org/10.15407/mfint.41.11.1455
37. H. Smithson, C.A. Marianetti, D. Morgan, A. Van der Ven, A. Predith, and G. Ceder, First-Principles Study of the Stability and Electronic Structure of Metal Hydrides, *Phys. Rev. B*, **66**, No. 12: 144107 (2002);
https://doi.org/10.1103/PhysRevB.66.144107
38. D.N. Movchan, V.N. Shyvanyuk, B.D. Shanina, and V.G. Gavriljuk, Atomic Interactions and Hydrogen-Induced γ^* Phase in FCC Iron–Nickel Alloys, *Phys. Status Solidi A*, **207**: 1796–1801 (2010);
https://doi.org/10.1002/pssa.200925548
39. H.Y. Mykhailova, V.A. Dekhtyarenko, and Y.V. Vasylyk, Hydrogen Sorption Properties of $Ti_{15.4}Zr_{30.2}Mn(_{54.4-x-y})V_xCr_yNi_y$ Alloy Able of Being Activated at Room Temperature and Pressure of 0.23 MPa, *MRS Communications*, **13**: 1288–1295 (2023);

https://doi.org/10.1557/s43579-023-00451-1
40. V.A. Dekhtyarenko, Composite Material Based on Laves Phase with Magnesium for Hydrogen Storage, *MRS Communications*, **14**: 337–344 (2024); https://doi.org/10.1557/s43579-024-00534-7
41. K.P. Gupta The Ni–Ti–Zr System (Nickel–Titanium–Zirconium), *J. Phase Equilibria*, **20**, No. 4: 441–448 (1999); https://doi.org/10.1361/105497199770335604
42. S.V. Mitrokhin, T.N. Bezuglaya, and V.N. Verbetsky, Structure and Hydrogen Sorption Properties of (Ti,Zr)–Mn–V Alloys, *J. Alloys Compd.*, **330–332**: 146–151 (2002); https://doi.org/10.1016/S0925-8388(01)01469-4
43. S.V. Mitrokhin, T.N. Smirnova, V.A. Somenkov, V.P. Glazkov, and V.N. Verbetsky, Structure of (Ti,Zr)–Mn–V Nonstoichiometric Laves Phases and $(Ti_{0.9}Zr_{0.1})(Mn_{0.75}V_{0.15}Ti_{0.1})_2D_{2.8}$ Deuteride, *J. Alloys Compd.*, **356–357**: 80–83 (2003); https://doi.org/10.1016/S0925-8388(03)00257-3
44. T.A. Zotov, V.N. Verbetskii, T.Ya. Safonova, A.V. Garshev, and O.A. Petriiz, Hydrogen Sorption and Electrochemical Properties of Alloys: Systems Zr–Ti–Ni–V–Mn with Laves Phase Structures, *Russ. J. Electrochem.*, **43**, No. 3: 355–363 (2007); https://doi.org/10.1134/S1023193507030147
45. F. Stein and A. Leineweber, Laves Phases: a Review of Their Functional and Structural Applications and an Improved Fundamental Understanding of Stability and Properties, *J Mater Sci.*, **56**: 5321–5427 (2021); https://doi.org/10.1007/s10853-020-05509-2
46. S.V. Mitrokhin, Regularities of Hydrogen Interaction with Multicomponent Ti(Zr)–Mn–V Laves Phase Alloys, *J. Alloys Compd.*, **404–406**: 384–387 (2005); https://doi.org/10.1016/j.jallcom.2005.02.078
47. V.A. Dekhtyarenko, Structure and Hydrogen Sorption Properties of $(Ti_{0.34}Zr_{0.66})Mn_{1.11}V_{0.1}$ Alloy, *Metallofiz. Noveishie Tekhnol.*, **37**, No. 5: 683–688 (2015) (in Russian); https://doi.org/10.15407/mfint.37.05.0683
48. T.V. Pryadko and V.A. Dekhtyarenko, Influence of Partial Substitution of Manganese with Chromium on Structure and Kinetics of Hydrogenation of an Alloy Based on the (Ti, Zr)$(V, Mn)_{2-x}$ Intermetallide, *Metallofiz. Noveishie Tekhnol.*, **40**, No. 5: 649–660 (2018) (in Russian); https://doi.org/10.15407/mfint.40.05.0649
49. N.N. Greenwood and A. Earnshaw, *Chemistry of the Elements* (Oxford: Butterworth Heinemann: 1997).
50. J.R. Johnson, Reaction of Hydrogen with the High Temperature (*C*14) form of $TiCr_2$, *J. Less-Common Met.*, **73**: 345–354 (1980); https://doi.org/10.1016/0022-5088(80)90328-8
51. J. Bodega, J.F. Fernández, F. Leardini, J.R. Ares, and C. Sánchez, Synthesis of Hexagonal *C*14/*C*36 and Cubic *C*15 $ZrCr_2$ Laves Phases and Thermodynamic Stability of Their Hydrides, *J. Phys. Chem. Solids*, **72** No. 11: 1334–1342 (2011); https://doi.org/10.1016/j.jpcs.2011.08.004
52. V. Ivanchenko, V. Dekhtyarenko, T. Kosorukova, and T. Pryadko, Phase Equilibria on the $TiMn_2$–$TiFe_2$, Polythermal Section, *Chem. Met. Alloys.*, **1**, No. 2: 137–139 (2008); https://doi.org/10.30970/cma1.0045
53. O.I. Dekhtyar, O.M. Ivasishin, D.Yu. Kovalev, O.M. Korduban, V.K. Prokudina, V.I. Ratnikov, D.G. Savvakin, A.Ye. Sychev, and M.M. Gumenyak, Features of Phase Formation at Controlled Hydrogenation and Dehydrogenation of Titanium by Dif-

ferent Methods, *Metallofiz. Noveishie Tekhnol.*, **36**, No. 9: 1153–1169 (2014) (in Russian);
https://doi.org/10.15407/mfint.36.09.1153

54. T.V. Pryadko, V.A. Dekhtyarenko, and A.A. Shkola, Influence of the Ambient Medium in the Course of Laser Treatment on the Resistance of Titanium to Hydrogen Embrittlement, *Mater Sci.*, **56**: 75–81 (2020);
https://doi.org/10.1007/s11003-020-00399-w
55. V.A. Dekhtyarenko, T.V. Pryadko, O.I. Boshko, V.V. Kirilchuk, H.Yu. Mykhailova, and V.I. Bondarchuk, Hydrogen Embrittlement of Titanium: Phenomena and Main Ways of Prevention, *Prog. Phys. Met.*, **25**, No. 2: 276–293 (2024);
https://doi.org/10.15407/ufm.25.02.276
56. V.A. Dekhtyarenko, T.V. Pryadko, D.G. Savvakin, V.I. Bondarchuk, and G.S. Mogylnyy, Hydrogenation Process in Multiphase Alloys of Ti–Zr–Mn–V System on the Example of $Ti_{42.75}Zr_{27}Mn_{20.25}V_{10}$ Alloy, *Int. J. Hydrogen Energy*, **46**: 8040–8047 (2021);
https://doi.org/10.1016/j.ijhydene.2020.11.283
57. K.B. Minko, M.V. Lototskyy, I.E. Bessarabskaya, and B.P. Tarasov, CFD simulation of heat and mass transfer processes in a metal hydride hydrogen storage system, taking into account changes in the bed structure, *Int. J. Hydrogen Energy* (2024);
https://doi.org/10.1016/j.ijhydene.2024.05.083
58. V.G. Gavriljuk, V.M. Shyvaniuk, and S.M. Teus, Hydrogen Embrittlement, *Hydrogen in Engineering Metallic Materials* (Springer: 2022), p. 201;
https://doi.org/10.1007/978-3-030-98550-9_5
59. V.A. Tatarenko and C.L. Tsynman, Strain-Induced and Blocking Effects in Thermodynamics of The Ordering and Precipitation Reactions within the Off-Stoichiometric Close-Packed-Metal Hydrides, *Solid State Ionics*, **101–103**, Pt. 1: 1061–1067 (1997);
https://doi.org/10.1016/s0167-2738(97)00376-7
60. V.A. Tatarenko and T.M. Radchenko, Direct and Indirect Methods of the Analysis of Interatomic Interaction and Kinetics of a Relaxation of the Short-Range Order in Close-Packed Substitutional (Interstitial) Solid Solutions, *Usp. Fiz. Met.*, **3**, No. 2: 111–236 (2002);
https://doi.org/10.15407/ufm.03.02.111
61. T.M. Radchenko, V.A. Tatarenko, H. Zapolsky, and D. Blavette, Statistical-Thermodynamic Description of the Order–Disorder Transformation of $D0_{19}$-Type Phase in Ti–Al Alloy, *J. Alloys Compd.*, **452**, No. 1: 122–126 (2008);
https://doi.org/10.1016/j.jallcom.2006.12.149
62. *Molecular Systems under High Pressure* (Eds. R. Pucci and G. Piccito) (Elsevier: 1991), p. 139–156.
63. M. Lototskyy, I. Tolj, Y. Klochko, M.W. Davids, D. Swanepoel, and V. Linkov, Metal Hydride Hydrogen Storage Tank for Fuel Cell Utility Vehicles, *Int. J. Hydrogen Energy*, **45**: 7958–7967 (2020);
https://doi.org/10.1016/j.ijhydene.2019.04.124
64. O.M. Ivasishin, D.G. Savvakin, M.M. Gumenyak, O.B. Bondarchuk, Role of Surface Contamination in Titanium PM, *Key Eng. Mater.*, **520**: 121–132 (2012);
https://doi.org/10.4028/www.scientific.net/KEM.520.121
65. S. Dong, G. Ma, P. Lei, T. Cheng, D. Savvakin, and O. Ivasishin, Comparative Study on the Densification Process of Different Titanium Powder, *Adv. Powder Technol.*, **32**: 2300–2310 (2021);
https://doi.org/10.1016/j.apt.2021.05.009
66. V.G. Ivanchenko, V.A. Dekhtyarenko, and T.V. Pryadko, Hydrogen-Sorption Prop-

erties of (Ti, Zr)Mn_{2-x} Intermetallic Alloy, *Powder Metall. Met. Ceram.*, **52**: 340–344 (2013);
https://doi.org/10.1007/s11106-013-9531-9
67. O.M. Ivasyshyn and D.H. Savvakin, Synthesis of Zirconium and Titanium-Based Alloys with the Use of Their Hydrides, *Mater. Sci.*, **51**: 465–474 (2016);
https://doi.org/10.1007/s11003-016-9863-y

Received 27.06.2024
Final version 30.10.2024

В.А. Дехтяренко[1,2], Т.В. Прядко[1], Т.П. Владімірова[1], С.В. Максимова[2], О.М. Семирга[1], В.І. Бондарчук[1]

[1] Інститут металофізики ім. Г.В. Курдюмова НАН України, бульв. Академіка Вернадського, 36, 03142 Київ, Україна
[2] Інститут електрозварювання ім. Є.О. Патона НАН України, вул. Казимира Малевича, 11, 03150 Київ, Україна

ВПЛИВ ЛЕГУВАННЯ НА ВОДНЕСОРБЦІЙНІ ВЛАСТИВОСТІ СПЛАВІВ НА ОСНОВІ Ti–Zr–Mn. Ч. 2: Евтектичні сплави з лавесовою фазою та структурою ОЦК-твердого розчину

Через огляд і аналіз літературних даних досліджено мікроструктуру та фазовий склад евтектичних сплавів $Ti_{47,5}Zr_{28}Mn_{(22,5-x)}V_2Ni_x$ (де x = 5,0 та 17,5 ат.%) у литому та відпаленому станах, а також фазовий склад продуктів гідрування, одержаних на їхній основі. Застосовано методи рентгенівського фазового аналізу та сканувальної електронної мікроскопії. Встановлено, що введений у сплав Нікель розподілився між ОЦК-твердим розчином та інтерметалідом з істотною перевагою на користь останнього. Крім того, визначено, що із заміною Мангану Нікелем від 5 до 17,5 ат.% відбулася зміна у фазовому складі вихідного сплаву: утворилася додаткова потрійна ψ-фаза NiTiZr, яка є ізоструктурною щодо лавесової фази (*C*14). Також показано, що для активації процесу вбирання H за кімнатної температури та тиску водню у 0,6 МПа критичним чинником є розмір кристалітів інтерметаліду. За площі поверхні зерен у 1–10 мкм^2 (для вихідної евтектичної структури) активна взаємодія сплаву з воднем під час першого гідрування відбувалася виключно під час нагрівання та впродовж ізобарно-ізотермічної витримки за температури у 510±10 °C, тоді як збільшення площі кристалітів до 100–300 мкм^2 завдяки відпалу уможливило початок цього процесу за кімнатної температури. Збільшення розмірів кожної із фазових складових спричинило більшу невідповідність об'ємних ефектів на міжфазних межах між сусідніми кристалами на початкових етапах гідрування, що призвело до руйнування поверхні сплаву з утворенням тріщин і подальшої активації взаємодії з воднем.

Ключові слова: Нікель, евтектика, ОЦК-твердий розчин, інтерметалід, гідрування, дегідрування, воднева місткість.